Thermochronology of high heat-producing crust at Mount Painter, South Australia: Implications for tectonic reactivation of continental interiors

Sandra McLaren,[1,2,3] W. James Dunlap,[4] Mike Sandiford,[5] and Ian McDougall[4]

Received 15 December 2000; revised 30 November 2001; accepted 13 December 2001; published XX Month 2002.

[1] The Mount Painter Region in the Northern Flinders Ranges, South Australia, contains a Mesoproterozoic gneissic complex characterized by extraordinary heat production (~16 μW m^{-3}), resulting in the development of elevated middle-upper crustal thermal gradients through much of the Paleozoic. Early Paleozoic deformation and metamorphism attained amphibolite facies (>500°C) in the deepest parts of the metamorphic pile (~10–12 km) during the ~500 Ma Cambro-Ordovician Delamerian orogeny. The subsequent thermal history of these rocks is assessed through new K/Ar and $^{40}Ar/^{39}Ar$ age measurements on amphiboles and micas and multiple-diffusion-domain thermal modeling of K-feldspar $^{40}Ar/^{39}Ar$ data. The preferred interpretation of these data is that the deepest rocks were at ~500°C until around 430 Ma, requiring average upper crustal thermal regimes of the order of 40°C km^{-1} for at least 70 million years. At around 430 Ma, and again at 400 Ma, the terrane underwent periods of moderately fast cooling, possibly separated by a period of isothermal residence. Following cooling at 400 Ma, the terrane entered a second period of relative tectonic quiescence remaining essentially isothermal until ~330 Ma. This long residence near the closure temperature of biotite resulted in variable argon loss from biotites in the 400 Ma to 330 Ma interval. Tectonic and thermal stability was terminated by a further period of moderately fast cooling (~4°–8°C Ma^{-1}) in the interval between 330 and 320 Ma. The three cooling episodes at around 430 Ma, 400 Ma, and 330 Ma are interpreted to be the result of exhumation resulting in a combined minimum of 6–7 km of denudation. We attribute this exhumation to the Alice Springs orogeny, a major intraplate tectonothermal event known throughout central Australia but not previously recognized as a significant tectonic event in the Adelaide Fold Belt. These new data provide compelling evidence that thermally modulated variations in lithospheric strength control the distribution of intraplate deformation at the continental scale. *INDEX TERMS:* 8110 Tectonophysics: Continental tectonics—general (0905); 1035 Geochemistry: Geochronology; 5134 Physical Properties of Rocks: Thermal properties; 8102 Tectonophysics: Continental contractional orogenic belts;

KEYWORDS: intraplate, tectonics, geochronology, radiogenic, Proterozoic, Palaeozoic

1. Introduction

[2] The distribution of active deformation in the interior of continents highlights the fact that proximity to active plate boundaries cannot be the sole determinant in shaping the tectonic response. For example, the heterogeneous partitioning of deformation in central Asia requires substantial variation in the mechanical properties of the Asian lithosphere [*Neil and Houseman*, 1997], and the flat-slab model for the Laramide orogeny [*Bird*, 1998] extends the locus of deformation many hundreds of kilometers inboard of the collisional boundary. The recognition of such heterogeneity raises critical questions such as what is the spatial and temporal amplitude of the mechanical variation in the continental lithosphere, what controls the spatial variations in mechanical response, and how does the mechanical response of the lithosphere change as a function of tectonic activity?

[3] Thermal regime is one of the most likely factors contributing to spatial and temporal variations in the mechanical response of the lithosphere [*England*, 1987; *Sonder and England*, 1986; *Zhou and Sandiford*, 1992]. The characteristic thermal regime of continental lithosphere is constrained by the global heat flow data set [*Pollack et al.*, 1993]. This data set suggests that approximately one half to two thirds of the average surface heat flow (~65 mW m^{-2}) is due to heat production within the lithosphere, with the remainder due to heat supplied by convective processes from beneath the lithosphere. The same data set also points to substantial regional variations in heat flow. For example, heat flow data from South Australia point to enrichment in heat-producing elements possibly by as much as a factor of 2 relative to normal continental crust [*Neumann et al.*, 2000]. One of the most extraordinary parts of this anomalous heat flow region in South Australia is at Mount Painter, in the northern Flinders Ranges, where Mesoproterozoic gneissic complexes exposed over a 100 km by 30 km wide zone, have an area-averaged heat production of ~16 μW m^{-3}, more than 3 times greater than the upper crustal average [*McLaren*, 2001]. Such extreme heat production values are consistent with the present-day heat flow of 120 mW m^{-2} [*Cull*, 1982] and suggest that crustal sources may contribute close to 100 mW m^{-2} to the surface heat flow. Despite apparently being located well within the continental interior from at least the Mesoproterozoic to the present day, this province records a long, complex, and ongoing record of deformation involving basin formation and inversion [*Sandiford et al.*, 1998; *Paul et al.*, 1999]. Modern thermochronological methods allow detailed reconstruction of thermal histories, which can be used to help understand the links

[1]Department of Geology and Geophysics, University of Adelaide, Adelaide University, SA, Australia.
[2]Also at School of Earth Sciences, University of Melbourne, Melbourne, Victoria, Australia.
[3]Now at Research School of Earth Sciences, Australian National University, Acton, ACT, Australia.
[4]Research School of Earth Sciences, Australian National University, Canberra, ACT, Australia.
[5]School of Earth Sciences, University of Melbourne, Melbourne, Victoria, Australia.

0278-7407/02/2000TC001275$12.00

between thermal regime and tectonic activity. To this end, this paper presents K/Ar and $^{40}Ar/^{39}Ar$ data, which, for the first time, allows the thermochronological record of the Mount Painter region to be constrained.

2. Geologic Setting

[4] The Adelaide Fold Belt in South Australia comprises deformed Neoproterozoic and Cambrian sediments of the Adelaide geosyncline [*Preiss*, 1987] overlying a Paleoproterozoic and Mesoproterozoic crystalline basement (timescale of *Young and Laurie* [1996], used throughout). The fold belt is subdivided into four main structural domains, the southern Adelaide Fold-Thrust Belt, the Nackara Arc, the central Flinders Ranges, and the Northern Flinders Ranges (Figure 1). The Mount Painter province (MPP), comprising the Mount Painter and Mount Babbage Inliers, forms the northernmost basement of the Adelaide Fold Belt system in the Northern Flinders Ranges (Figure 1). The eastern margin of the Northern Flinders Ranges coincides with the Paralana fault, along which the MPP is thrust over the adjacent Curnamona craton. The western margin of the northern Flinders Ranges is marked by the Norwest fault and to the north lie the Paleozoic Warburton, Cooper, and Eromanga basins (Figure 1).

[5] In the MPP the Mount Painter and Mount Babbage inliers consist of metasediments that were deposited and metamorphosed at high-grade conditions during the Paleoproterozoic [*Teale*, 1993], and subsequently intruded by Mesoproterozoic granites. These units are overlain by a ~7–12 km thick Neoproterozoic sedimentary sequence forming part of the Adelaide geosyncline (Figure 2). This sedimentary cover was deposited between ~830 and 550 Ma [*Preiss*, 1987, 2000] during a sequence of rift-related subsidence events. Subsequent deformation and metamorphism, the subject of this paper, affected both the basement and the cover.

[6] In the Southern Adelaide Fold Belt (Figure 1), U-Pb zircon data from synkinematic and postkinematic granites constrain the timing of this deformation and metamorphism to between 515 and 490 Ma [*Jenkins and Sandiford*, 1992; *Foden et al.*, 1999], an event termed the Delamerian orogeny. Tectonism throughout the remainder of the Adelaide Fold Belt, including at Mount Painter, is also ascribed to this event, largely on the basis of a similarity in structural style, and a predeformational depositional record which everywhere terminates at about the same time in the Early Cambrian [*Jenkins and Sandiford*, 1992]. In the Mount Painter region, however, we can only be certain that the deformation occurred subsequent to ~550 Ma, the approximate depositional age of the youngest deformed sediments overlying the basement.The Paleozoic deformation is typically thick skinned, basement involved, and is characterized by the propagation of large-amplitude, basement-cored upright folds which plunge gently to the southwest (Figure 3). The basement cover unconformity is folded on the regional scale, and total shortening is estimated at ~20% [*Paul et al.*, 1999]. The main fabric formed at high-temperature low-pressure conditions. Isograds in the lower part of the cover succession are essentially concordant with the basement unconformity (Figure 3b), defining an unusual style of "unconformity-related contact metamorphism" [*Mildren and Sandiford*, 1995; *Sandiford et al.*, 1998]. The occurrence of cordierite-anthophyllite and diopside-bearing rocks immediately above the basement cover unconformity

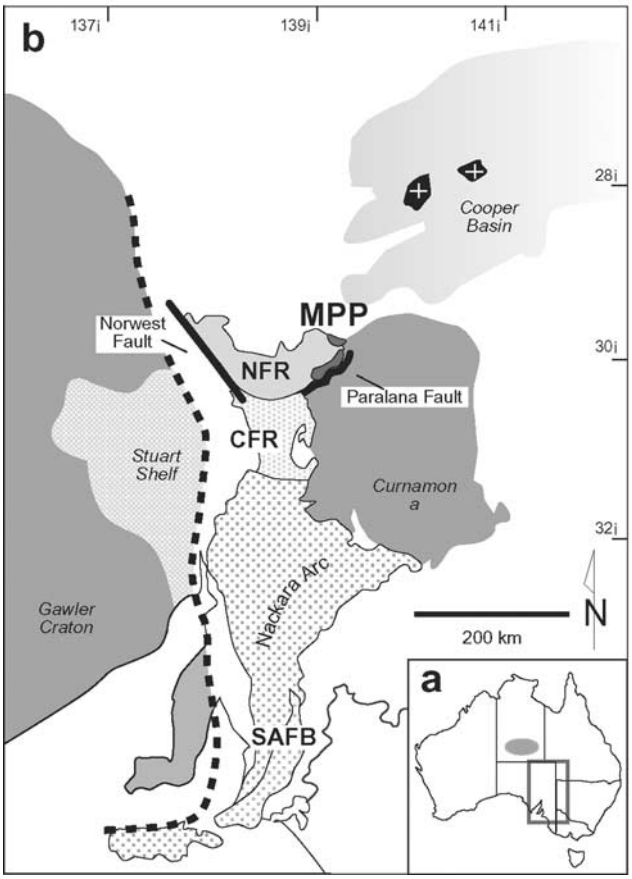

Figure 1. (a) Location of the Adelaide Fold Belt within South Australia. Area of central Australia affected by the Alice Springs orogeny (ASO) shown as gray stipple. (b) Structural framework of northern and central South Australia. The region shown in light stipple is the Adelaide Fold Belt, including the Southern Adelaide Fold-Thrust Belt (SAFB), the Nackara Arc, the Central Flinders Ranges (CFR), and the Northern Flinders Ranges (NFR). The Mount Painter province (MPP) is shown by the darkest shading. Also shown are the inferred extents of the Proterozoic Curnamona and Gawler cratons and the late Carboniferous-Triassic Cooper Basin. The Warburton Basin underlies the Cooper Basin and is intruded by ~300 Ma granites.

suggests peak metamorphic temperatures of at least 500°C. Pressures are estimated to be ~3 kbar from the widespread association of cordierite-biotite-muscovite, equating to a depth of ~12 km assuming an average density of 2500 kg m^{-3} for the covering sediments. These data imply an average upper crustal thermal gradient of ~40°C km^{-1} [*Sandiford et al.*, 1998]. There is no evidence that the sequence has been buried to depths significantly greater than the 12 km recorded by the prograde mineral assemblages, suggesting that the principal contribution to burial was the accumulation of the Neoproterozoic sedimentary basin [*Paul et al.*, 1999].

[7] Although the timing of the Paleozoic deformation and metamorphism can be loosely constrained to be younger than 550 Ma, the cause of this metamorphism is less clear. There are no mafic intrusives postdating the Wooltana Volcanics (at the base of the Adelaidean sequence), and although there are a number of

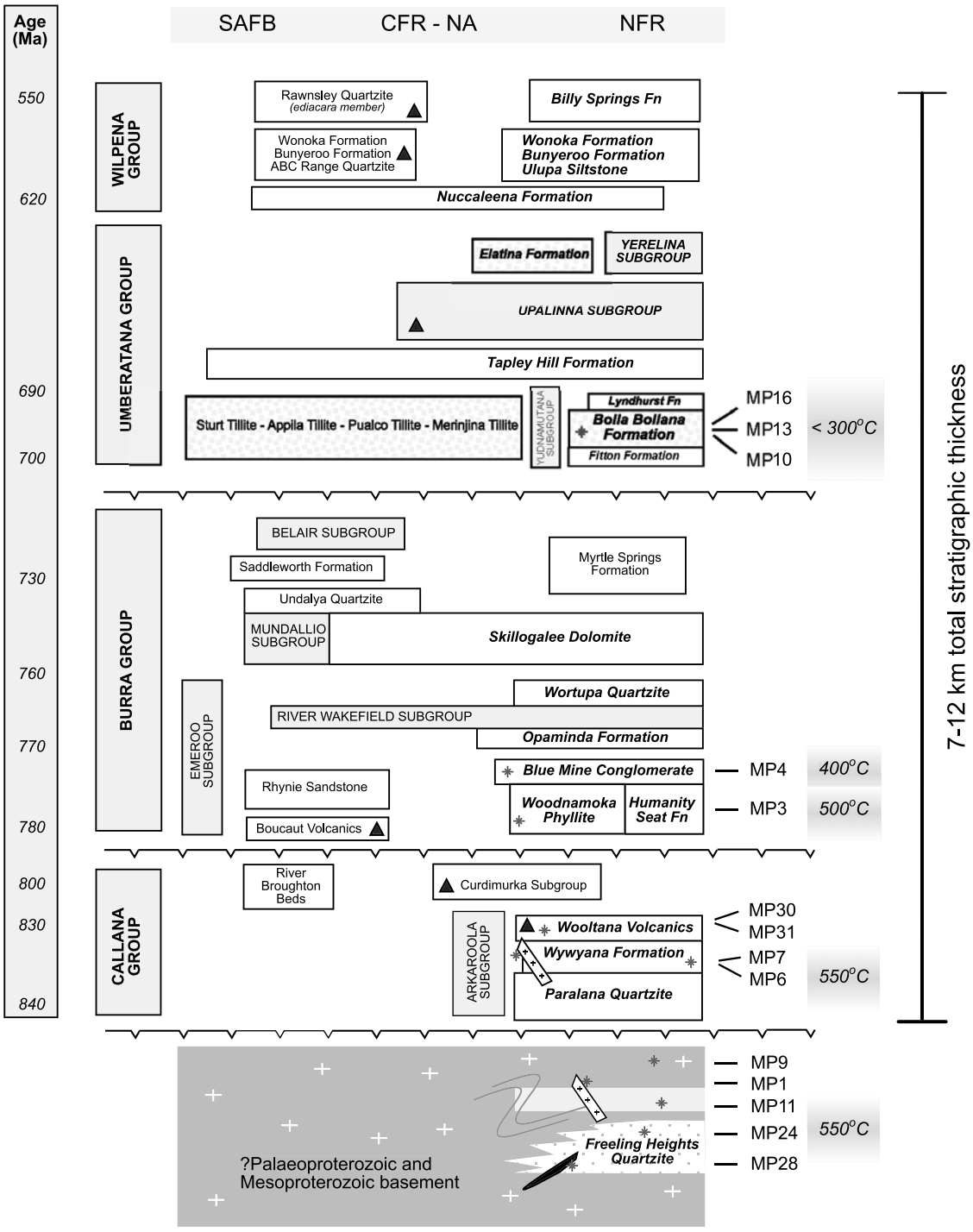

Figure 2. Generalized stratigraphy of the Adelaidean cover sequence in the SAFB, CFR, and NA, and the NFR. Italicized units outcrop in the Mount Painter region. Stratigraphic units denoted with an asterisk were sampled for potassium-argon analysis, with sample numbers listed to show relative stratigraphic position. Position of Paleozoic pegmatites is also shown. Estimated peak Paleozoic metamorphic temperatures are indicated. Units denoted with a triangle have been subject to age determinations, with these data largely SHRIMP U/Pb ages from zircons within crosscutting dykes or interleaved tuffs [*Preiss*, 2000]. Stratigraphic relations adapted from *Preiss* [1987, 2000]; age column on the left indicates estimated depositional age, after *Preiss* [2000]. Toothed lines denote major unconformities.

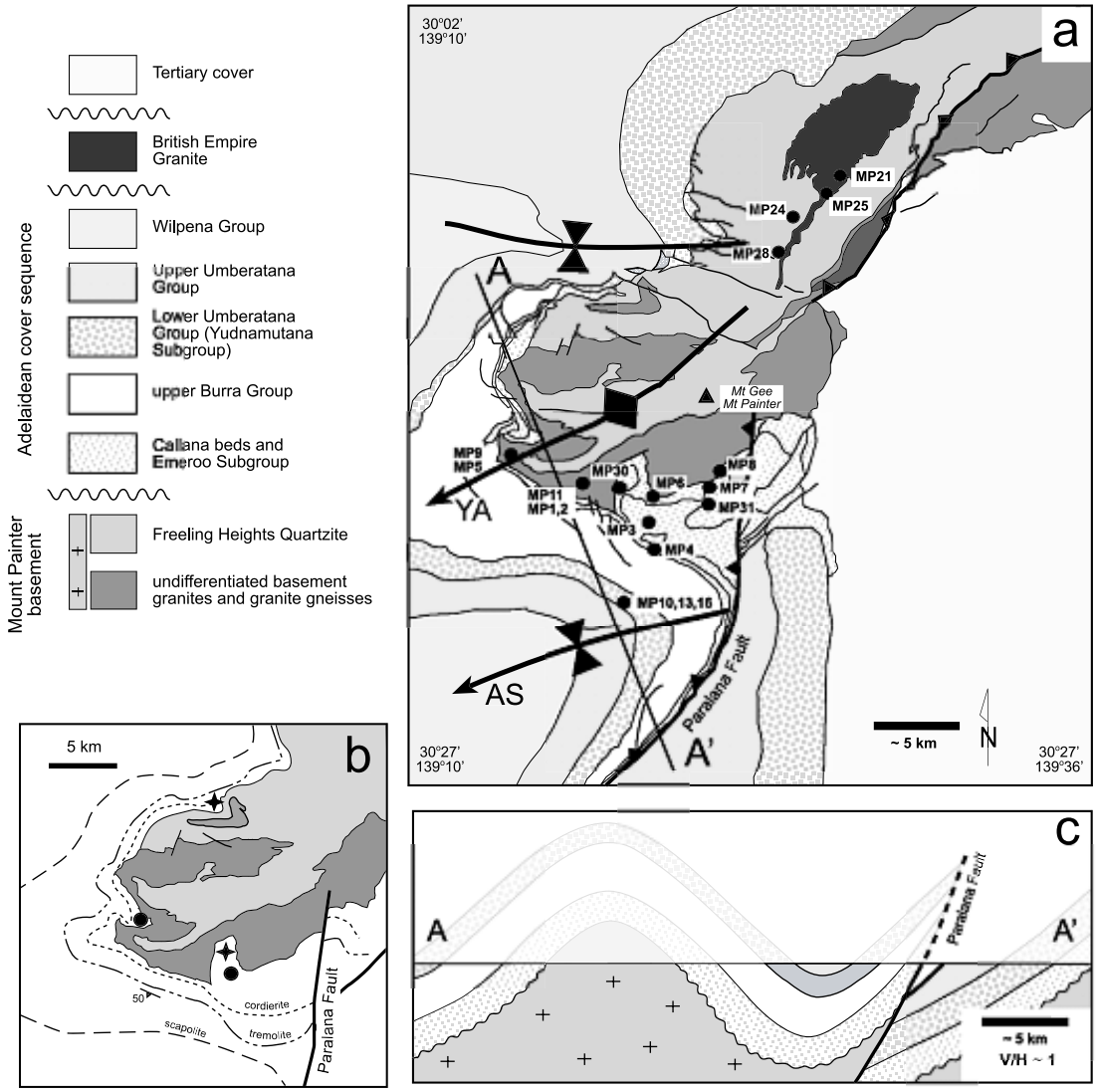

Figure 3. (a) Geology of the southern Mount Painter inlier showing sample locations. Geology modified from *Coats et al.* [1969] and shown by stratigraphic group only; YA, Yankannina Anticline; AS, Arkaroola Syncline [*Paul et al.*, 1999]. (b) Section of map from Figure 3a illustrating the concordance of metamorphic isograds with the basement cover unconformity. Circles show diopside localities and stars show cordierite-anthophyllite assemblages. (c) Schematic cross section through the southern Mount Painter inlier illustrating general structural style. Section is drawn at approximately the same scale as map view, with no vertical exaggeration [*Paul et al.*, 1999].

small Paleozoic pegmatoidal bodies (including the British Empire Granite; Figure 3), these are considered to be a consequence rather than a cause of the metamorphism. These observations suggest that transient models for high- temperature low-pressure metamorphism [*De Yoreo et al.*, 1991; *Karlstrom and Williams*, 1995] do not apply. However, the Proterozoic basement units in the Mount Painter inlier are extraordinarily enriched in the heat-producing elements and contribute as much as 100 mW m^{-2} to the surface heat flow. In a model that accounts for both metamorphic pressures and known sediment thicknesses, *Sandiford et al.* [1998] suggested that the metamorphic conditions may primarily reflect the burial of high–heat-producing Proterozoic basement beneath the cover sequence during a period of extended thermal subsidence. A first-order prediction of this conductive model is that temperature and depth are correlated, and only when the rocks are exhumed should they be cooled.

[8] A number of lines of evidence suggest that significant tectonic activity continued after the Delamerian orogeny in both the Mount Painter region and in adjacent crustal blocks. Whole rock Rb-Sr isotopic ages of ~450–350 Ma for basement granites and gneisses [*Neumann*, 1996; *Schaefer*, 1993] and K/Ar age determinations on six biotite separates from the Yerila Granite, in the Mount Babbage inlier, of around 400 Ma (A. W. Webb, unpublished report, 1976), suggest that the Mount Painter rocks remained above ~300°C for a considerable time following the Delamerian orogeny. The timing of the final exhumation is con-

strained by ~260–175 Ma apatite fission track ages [*Foster et al.*, 1994]. In the Warburton-Cooper Basin to the north, ~298 and 323 Ma granitoids [*Gatehouse et al.*, 1995] are indicative of crustal disturbances extending toward central Australia, where Carboniferous intraplate tectonism and magmatism are well known [*Dunlap and Teyssier*, 1995].

3. K/Ar and $^{40}Ar/^{39}Ar$ Analysis

[9] Potassium-rich minerals have a large range of closure temperature, T_c [*Dodson*, 1973] with respect to the accumulation of radiogenic argon; hornblende ~500°C [*Harrison*, 1981]; muscovite ~350°C [*Hames and Bowring*, 1994]; biotite ~300°C, [*Harrison et al.*, 1985]; and K-feldspar closes over the 350°C to 150°C range [*Lovera et al.*, 1989]. Synthesis of data allows a cooling history to be elucidated because of the different closure temperatures. K/Ar and $^{40}Ar/^{39}Ar$ isotopic analyses were performed on 19 mineral separates from both Mesoproterozoic, or older, basement rocks and the overlying Neoproterozoic Adelaidean cover sequence (Table 1; Figures 2 and 3a). The analytical methods employed are summarized in Appendix A and by *McDougall and Harrison* [1999]. In this discussion we use the term "plateau" for that part of an age spectrum where the ages of consecutive steps are within 2σ of one another and together comprise at least 50% of the gas release. We also apply the term "plateau-like" if one or two steps in such a sequence are discordant.

3.1. Hornblendes

[10] Three hornblende mineral separates, from samples MP30, MP31, and MP28, were analyzed using the K/Ar and $^{40}Ar/^{39}Ar$ techniques. Sample MP30 is a hornblende, plagioclase- and actinolite-bearing metabasalt from the Wooltana Volcanics (Figure 2) adjacent to the basement cover unconformity. This sample yields an apparent K/Ar age of 395 ± 4 Ma (Table 2) and a highly disturbed age spectrum (Figure 4). The mineral separate appears to contain ~5% K-feldspar, and this component contains much of the K, judging from the descending K/Ca values during $^{40}Ar/^{39}Ar$ analysis. On the basis of this contamination we do not include this analysis in further interpretation. Sample MP31, also from the Wooltana Volcanics and containing both hornblende and epidote, yields an apparent K/Ar age of 436 ± 5 Ma and a slightly disturbed age spectrum with a total gas age of 467 ± 5 Ma (Figure 4). The K/Ar analysis is discounted, however, as its low percentage of radiogenic argon (Table 2) possibly reflects a leak in the extraction line, which may bias the age to younger values. Ages in the spectrum range from around 445 to 500 Ma. A plateau like segment yields an age of 446 ± 1 Ma. Hornblende from sample MP28, an amphibolite dyke intruding basement rocks of the Freeling Heights Quartzite in the central Mount Painter inlier [*Neumann*, 1996], yields an apparent K/Ar age of 423 ± 6 Ma, and a very well-defined $^{40}Ar/^{39}Ar$ plateau age of 432 ± 1 Ma (Figure 4).

3.2. Muscovites and Biotites

[11] Potassium-argon results for both muscovite and biotite separates from metasediments and granite gneisses reveal a wide range of ages between 362 Ma and 407 Ma and 344 Ma and 399 Ma, respectively (Table 2). The apparent ages are considerably younger than the MP31 and MP28 hornblendes and show that mica samples experienced significant argon loss after formation during the Delamerian orogeny. Step heating experiments were performed on four of the nine muscovite samples in the K/Ar study, and on six of the seven biotite samples (Table 3). In general, there is close agreement between $^{40}Ar/^{39}Ar$ integrated total gas ages and K/Ar ages (Table 3). Isochron analysis did not give any additional useful information, as the samples are highly radiogenic.

[12] Biotite samples (excepting MP24) show flat plateau segments, in many cases for more than 90% of the gas release. Age spectra for muscovite samples show similar plateau features, for 80–90% of the gas release (Figure 4). Total gas and plateau ages for muscovite samples show remarkable consistency with stratigraphic and structural position, increasing in age toward the top of the metamorphic pile (Figure 4). A similar trend is seen among the biotite samples; however, MP2 is anomalously young for its structural position, whereas MP9 is anomalously old.

[13] Muscovite from sample MP24 gives a $^{40}Ar/^{39}Ar$ plateau age of 375 ± 2 Ma, whereas the total gas age for the biotite is 351 ± 3 Ma. The biotite age spectrum is strongly disturbed (Figure 4) and no plateau-like age is achieved. The mineral separate contains mostly green biotite, but brown biotite composed 10% of the mode. We speculate that brown biotite may be relatively more retentive, and that the hump shape of the age spectrum may be the result of differential release of argon during step heating [*Wijbrans and McDougall*, 1988]. This second phase of the gas release (>0.65) is characterized by much more variable K/Ca values.

[14] Biotite MP11 yields an age spectrum that is flat throughout the gas release, yielding a plateau age of 381 ± 2 Ma. The MP11 muscovite age spectrum is not as flat, exhibiting a range of ages from 382 Ma in the third step to 400 Ma in the last step, and a plateau-like age of 391 ± 2 Ma.

[15] The $^{40}Ar/^{39}Ar$ integrated total gas age for the MP9 biotite is 396 ± 2 Ma, and a plateau-like segment gives 401 ± 1 Ma (note age variation is not reflected in the error); muscovite from MP9 yields a slightly younger K/Ar age of 396 ± 3 Ma. The age spectrum from biotite MP9 is disturbed, however, exhibiting a pattern similar to that of biotite MP24 (Figure 4). Muscovite from sample MP5, a pegmatite which cuts the MP9 rocks, has a $^{40}Ar/^{39}Ar$ integrated total gas age of 392 ± 2 Ma; this age spectrum is nearly flat, with ages ranging from 384 Ma in the second step to 400 Ma in the last step. Although muscovites at this site are slightly younger than the biotite, when the uncertainties are taken into account the difference is not significant.

[16] Sample MP2 is a monomineralic biotite selvedge from adjacent to a K-feldspar pegmatite which is probably Paleozoic in age. The age spectrum is remarkably flat, yielding a plateau age of 365 ± 2 Ma. This sample is considerably younger than other biotite samples from equivalent structural positions (Tables 2 and 3), and this may be due to intrusion of the MP1 pegmatite (see MP1 K-feldspar results below).

[17] Biotite from sample MP7 shows good agreement between the measured K/Ar age and the $^{40}Ar/^{39}Ar$ integrated total gas age (374 ± 2 Ma). The gas release also defines a plateau age 374 ± 2 Ma.

[18] Biotite and muscovite from sample MP3 record the oldest ages of the micas, consistent with their high structural position. The biotite yields a plateau age of 387 ± 2 Ma, whereas the

Table 1. Sample Location and Description[a]

Sample	MU	BT	K-SPAR	HBDE	Lithology	Unit	Easting	Northing	Distance From Unconformity, km	Description
MP21	#		#		British Empire Granite	PG	350370	6666840	−2.0	coarse leucogranite, plagioclase, muscovite, quartzite, and microcline bearing
MP25	#	#			British Empire Granite	PG	349240	6665870	−2.0	coarse-grained, plagioclase-, muscovite-, biotite-, and quartzite-bearing granodiorite
MP24	x	x	x		Freeling Heights quartzite	MB	347250	6663400	−2.0	strongly foliated and recrystallized quartzite, foliation defined by muscovite and biotite
MP28				x	amphibolite	MB	346550	6661900	−2.0	recrystallized hornblende, biotite amphibolite
MP11	x	x			metasediment	MB	335164	6649213	−0.5	metasedimentary enclave within MB, strongly foliated and crenulated, foliation defined by muscovite and biotite
MP2		x			Nooldoonooldoona pegmatite	MB	335200	6649600	−0.5	metasomatized margin of local pegmatite; monomineralic, foliated biotite aggregate
MP9	#	x	x		foliated gneiss	MB	331125	6650867	−0.2	foliated muscovite, biotite gneiss
MP5	x				Arkaroola pegmatite	PG	330937	6650837	−0.2	deformed, coarse grained K-feldspar, muscovite pegmatite
MP8	#		#		Arkaroola Pegmatite	PG	341924	6649759	0	megacrystic K-feldspar, muscovite, quartzite, tourmaline pegmatite
MP1		x	x		Nooldoonooldoona pegmatite	PG	335200	6649600	+0.5	local K-feldspar pegmatite
MP6	#		x		Arkaroola pegmatite	PG	339617	6648145	+0.5	coarse, relatively undeformed K-feld spar, muscovite and diopside-bearing pegmatite
MP30				x	Wooltana Volcanics	ACS	337550	6649000	+0.5	hornblende, plagioclase metabasalt
MP7		x			local biotite schist	ACS	341934	6649855	+0.5	monomineralic biotite schist, associated with andalusite-bearing schist
MP31				x	Wooltana Volcanics	ACS	342550	6648750	+0.6	hornblende, epidote metabasalt
MP3	x	x			Woodnamoka phyllite	ACS	340250	6646550	+1.75	fine-grained sandy schist
MP4			x		Blue Mine Conglomerate	ACS	340050	6645550	+2.0	K-feldspar clast in arkosic conglomerate
MP10			x		Bolla Bollana Formation	ACS	337500	6643340	+3.0	granite clast within glacial tillite
MP13			#		Bolla Bollana Formation	ACS	337491	6642838	+3.0	granite clast within glacial tillite
MP16			x		Bolla Bollana Formation	ACS	337648	6642345	+3.0	porphyritic volcanic clast within glacial tillite

[a]Sample locations are given in Australian Map Grid (1984), zone 54. Petrological and thermal constraints on samples are given in the online data repository. Abbreviations are as follows: MU, muscovite, BT, biotite, K-SPAR, K-feldspar, HBDE, horneblende; MB, Mesoproterozoic Mount Painter Basement; ACS, Neoproterozoic Adelaidean Cover Sequence; PG, Paleozoic granite/pegmatite. Distances are quoted above (denoted positive) and below (denoted negative) the basement cover unconformity. Mineral separates denoted by an "x" were analyzed by both K/Ar and $^{40}Ar/^{39}Ar$ methods; separates denoted by a number symbol were analyzed by the K/Ar method only.

muscovite plateau-like segment is considerably older at 404 ± 2 Ma (Figure 4).

3.3. K-Feldspars

[19] Twelve K-feldspar samples were analyzed by the K/Ar method, and seven of these samples were also subjected to $^{40}Ar/^{39}Ar$ step heating experiments. The K/Ar data reveal a wide spread in apparent age (Table 2). The youngest samples are from pegmatites which are thought to have intruded during Paleozoic metamorphism. The oldest apparent ages are recorded in the Blue Mine Conglomerate and Bolla Bollana Formation, the highest stratigraphic units sampled. The agreement between K/Ar apparent ages and $^{40}Ar/^{39}Ar$ integrated total gas ages is good (Table 4); however, in three cases the K/Ar ages are a few percent younger, possibly due to incomplete argon extraction during the K/Ar age measurement.

[20] K-feldspar $^{40}Ar/^{39}Ar$ age spectra (Figure 5) are generally characterized by increasing ages (as temperature is raised), with the steepest age gradients occurring over the first 20% of the gas release. All spectra, regardless of stratigraphic or structural position, rise to ages between 330 and 450 Ma, indicating that the K-feldspars experienced significant post-Delamerian argon loss. Those samples which are not expected to have retained a Proterozoic prehistory, and which have clearly suffered high temperature metamorphism, exhibit a remarkably narrow range of ages. For samples MP1, MP6, and MP9, these plateau-like ages are all ~330 Ma. Samples MP4, MP10, and MP16 give slightly more complicated age spectra, with evidence of excess argon in the early released gas (Figure 5), as indicated by large differences in the age of isothermal duplicate steps (MP4 especially), or by a somewhat irregular shape (MP16).

3.3.1. Multiple diffusion domain analysis of K-feldspars. [21] We have interpreted the K-feldspar age spectra using the multiple-diffusion-domain (MDD) method described by *Lovera et al.* [1989] and *Richter et al.* [1991]. This method assumes that the release of argon is by a thermally activated diffusion process

Table 2. Results of K/Ar Isotopic Analyses[a]

Sample	Lithology	Unit	Mineral	K, wt %	Rad ^{40}Ar*, 10^{-9} mol/g	100 ^{40}Ar*/ Total ^{40}Ar	Calculated Age, Ma ± 1σ
MP21	British Empire Granite	PG	K-feldspar	12.46, 12.55	8.354	96.9	349.2 ± 2.8
			muscovite	8.827, 8.837	6.767	98.5	395.1 ± 3.1
MP25	British Empire Granite	PG	biotite	7.395, 7.421	5.211	77.2	365.8 ± 3.0
			muscovite	8.845, 8.812	6.546	76.9	383.6 ± 3.0
MP24	Freeling Heights Quartzite	MB	K-feldspar	12.51, 12.49	7.688	97.7	323.7 ± 2.5
			biotite	7.933, 7.950	5.219	82.5	343.9 ± 2.7
			muscovite	8.914, 8.964	6.492	94.3	376.5 ± 3.2
MP28	Amphibolite	MB	hornblende	0.451, 0.458	0.375	95.9	422.5 ± 6.1
MP9	basement gneiss	MB	K-feldspar	11.92, 11.92	7.767	93.6	341.3 ± 2.6
			biotite	8.325, 8.269	6.421	84.1	398.7 ± 3.2
			muscovite	9.056, 8.979	6.921	98.4	395.7 ± 3.1
MP11	basement metasediment	MB	muscovite	8.479, 8.417	6.490	79.7	396.1 ± 3.2
			biotite	8.490, 8.538	6.306	99.1	383.3 ± 3.2
MP8	Arkaroola Pegmatite	PG	K-feldspar	11.21, 11.36	6.944	88.2	323.9 ± 2.6
			muscovite	9.069, 8.955	6.286	97.0	363.0 ± 2.9
MP5	Arkaroola Pegmatite	PG	K-feldspar	11.08, 11.07	6.886	86.2	327.0 ± 3.9
			muscovite	8.983, 8.954	6.789	88.1	390.9 ± 3.0
MP1	local pegmatite	PG	K-feldspar	13.33, 13.39	8.207	96.1	323.4 ± 2.5
MP2	biotite schist	MB	biotite	8.248, 8.319	5.909	96.6	370.5 ± 2.9
MP6	Arkaroola Pegmatite	PG	K-feldspar	12.67, 12.66	8.079	93.4	334.6 ± 2.8
			muscovite	9.070, 9.063	6.296	88.2	361.6 ± 2.8
MP30	Wooltana Volcanics	ACS	hornblende	0.294, 0.294	0.2254	91.3	395.3 ± 4.2
MP31	Wooltana Volcanics	ACS	hornblende	0.312, 0.313	0.2666	51.8	435.5 ± 5.1
MP7	biotite Schist	ACS	biotite	8.336, 8.321	6.086	88.7	378.6 ± 3.0
MP3	Woodnamoka Phyllite	ACS	biotite	8.071, 8.153	6.062	79.9	386.3 ± 3.1
			muscovite	8.382, 8.287	6.606	95.8	407.3 ± 3.2
MP4	Blue Mine Conglomerate	ACS	K-feldspar	12.33, 12.34	8.712	66.6	367.2 ± 2.9
MP10	Bolla Bollana Formation	ACS	K-feldspar	11.67, 11.62	8.749	90.0	388.3 ± 3.1
MP13	Bolla Bollana Formation	ACS	K-feldspar	10.06 (x = 4)	11.77	97.1	573.3 ± 6.1
MP16	Bolla Bollana Formation	ACS	K-feldspar	8.572, 8.535	5.912	92.2	360.1 ± 3.0

[a]An age determination was made on each of two separate aliquots of argon from each sample. As these duplicate analyses were in good agreement, only one analysis is listed here. A complete listing is given in the electronic supporting material.

which can be described by the Arrhenius equation. Following *Lovera et al.* [1989], we calculated a single activation energy (E_a) and assume a slab geometry to calculate the distribution of diffusion domain length scales (volume fraction and effective size). The calculated domain distribution was then inverted to yield temperature-time histories, again following *Lovera et al.* [1989] and *Lovera et al.* [1997]. Temperature-time paths were calculated by inputting trial thermal histories and minimizing the differences between the laboratory and modeled age spectra by iteration. In many cases, application of the laboratory heating schedules result in model gas release histories that are almost identical to that obtained during the step heating experiments (Figure 5). Uncertainties in model temperatures are about ± 25°C (because of the uncertainty in E_a), assuming that the distribution of argon is diffusion controlled.

[22] We are able to model the laboratory age spectra using two end-member types of thermal histories: (1) continuous cooling and (2) thermal spikes; these two cases are thermally indistinguishable. For the Mount Painter samples a continuous cooling history is preferred as the geology suggests a simple post-Delamerian exhumation history. Note that the K-feldspar thermal models are strictly applicable only for ages less than the maximum age recorded by each sample, and in all but one case these ages are <400 Ma. As this is also the time of muscovite closure, it seems unlikely that any significant (> ~450°C) thermal pulses occurred from this time until the present. The MP1 and MP6 pegmatites, however, may have intruded as late as 360 Ma, so that we do not impose any prehistory on these samples (i.e., in all cases we do not try to model ages older than the maximum age of the samples).

3.3.2. Thermal modeling of K-feldspar data. [23] In developing the K-feldspar thermal models the first constraint is provided by the hornblende age data. Assuming that the closure temperature of hornblende to argon loss is ≥450°C [*Harrison*, 1981], we suggest that rocks from both the basement and cover sequences underwent a period of accelerated cooling from temperatures of at least 450°C at around 430 Ma, the time of final hornblende closure. Given that K-feldspars are significantly less retentive of their argon, all the K-feldspars, with the possible exception of those high in the cover sequence (e.g., MP10), should have been completely outgassed of any previously accumulated radiogenic argon at this time.

[24] The best fit thermal models show remarkable similarities. The general style of thermal evolution is common for all samples, regardless of structural or stratigraphic position. Good model fits are consistent with a period of rapid cooling at ~400 Ma, followed by a period of isothermal residence between ~390 and 330–325 Ma. A second period of rapid cooling at ~325 Ma is required by all samples to facilitate the closure of the smallest diffusion domains. In the remainder of this section we describe the thermal models for each group of K-feldspar samples, i.e., basement samples, Paleozoic intrusives, and cover sequence samples. The purpose of this discussion is to describe the times and temperatures at which changes in cooling rate are observed. These models, along with the K/Ar and

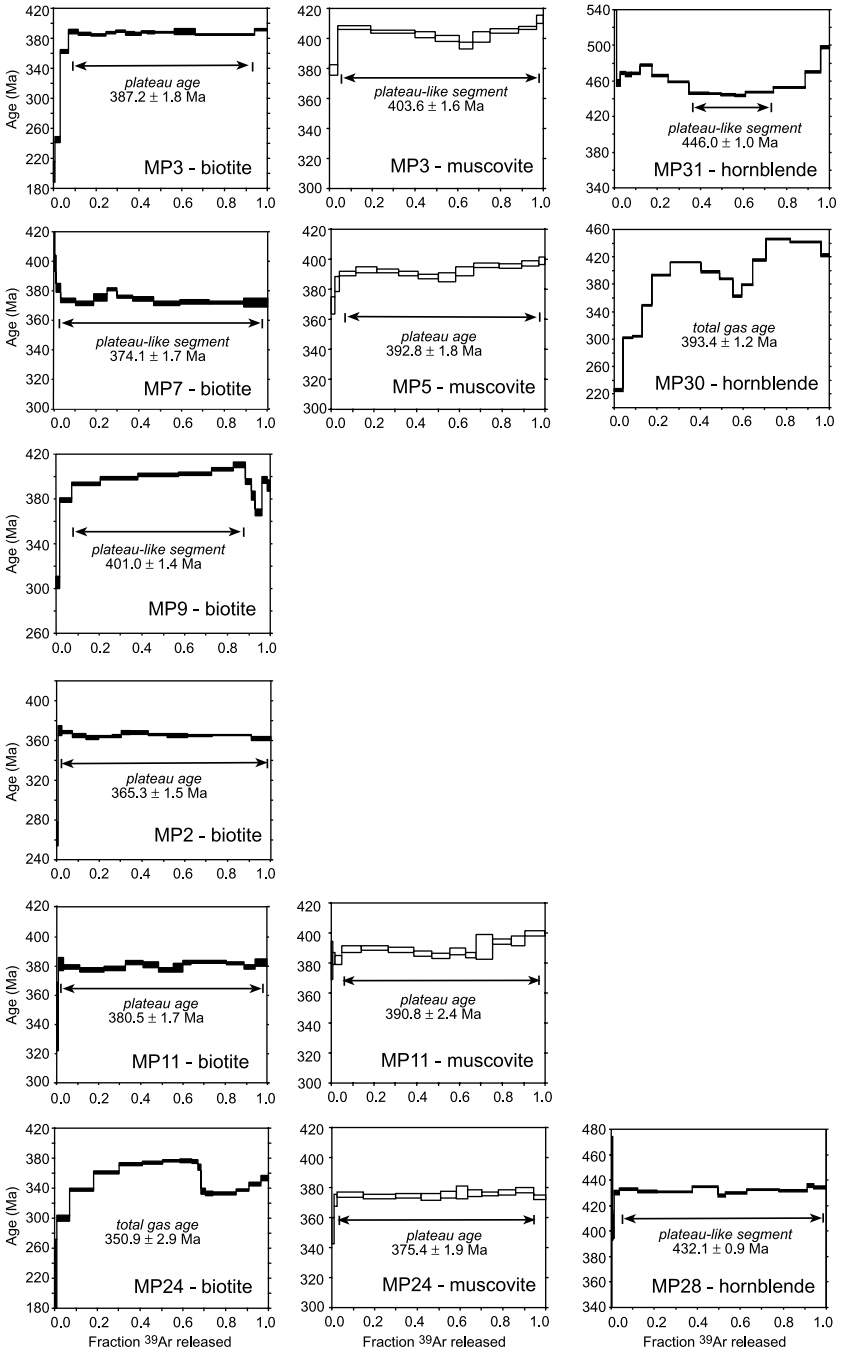

Figure 4. Summary of $^{40}Ar/^{39}Ar$ age spectra for hornblende, muscovite, and biotite samples. Spectra are arranged according to stratigraphic position, from the highest sample (MP3) to the lowest (MP24).

$^{40}Ar/^{39}Ar$ age measurements from micas and amphiboles, allow a model for the tectonic evolution to be developed.

[25] Samples MP24 and MP9 yield similar thermal histories, despite differences in their age spectra. Apparent ages in the range 250–340 Ma are recorded by sample MP9, whereas sample MP24 records higher apparent ages in the range 305–380 Ma. The hump-shape of the age spectrum from 5–15% gas release for sample MP9 suggests that the sample may contain minor excess argon, and this portion of the age spectrum cannot be fitted. Although both models are consistent with a period of rapid cooling at ~400 Ma, the absence of ages older than 380 Ma mean that neither bear on this issue directly. However, good model fits are obtained for a period of isothermal residence between around 380 Ma and 350 Ma. Unlike the other samples studied here, samples MP24 and MP9 suggest monotonic cooling throughout the period 350–300 Ma. Sample MP9 cools from about 320°C at 350 Ma; sample MP24 from 350°C, which is consistent with the deeper structural and stratigraphic position of sample MP24.

Table 3. Summary of Muscovite and Biotite K/Ar and $^{40}Ar/^{39}Ar$ Data

Sample	Mineral	K/Ar Age, Ma ± 1σ	Integrated Total Fusion $^{40}Ar/^{39}Ar$ Age, Ma ± 1σ	Plateau Age, Ma ± 1σ
MP28	hornblende	422.5 ± 6.1	431.3 ± 1.1	432.1 ± 0.9
MP30	hornblende	395.3 ± 4.2	393.4 ± 1.2	–
MP31	hornblende	435.5 ± 5.1	467.0 ± 1.2	446.0 ± 1.0
MP24	muscovite	376.5 ± 3.2	374.8 ± 2.0	375.4 ± 1.9
MP11	muscovite	396.1 ± 3.2	389.9 ± 2.6	390.8 ± 2.4
MP5	muscovite	390.9 ± 3.0	391.8 ± 2.0	392.8 ± 1.8
MP3	muscovite	407.3 ± 3.2	402.9 ± 2.0	403.6 ± 1.6
MP24	biotite	343.9 ± 2.9	350.9 ± 2.9	–
MP11	biotite	383.3 ± 3.2	379.8 ± 2.0	380.5 ± 1.7
MP9	biotite	398.7 ± 3.2	395.9 ± 2.0	401.0 ± 1.4
MP2	biotite	371.2 ± 3.0	363.8 ± 1.7	365.3 ± 1.5
MP7	biotite	378.3 ± 3.0	373.7 ± 1.7	374.1 ± 1.7
MP3	biotite	386.3 ± 3.1	380.2 ± 2.2	387.2 ± 1.8

[26] K-feldspars MP10 and MP16 were both sampled from boulder clasts within the Bolla Bollana Formation, a glacial tillite (Figure 2). MP10 is from a granitic clast, whereas MP16 is from a volcanic clast. Both samples show pronounced monotonically rising age spectra. The age spectrum of MP10 suggests that it started to accumulate argon before 440 Ma, with final closure of the smallest diffusion domains occurring around 310 Ma. The 440 Ma apparent ages are similar to the $^{40}Ar/^{39}Ar$ ages of MP31 and MP28 amphiboles and together suggest a period of cooling at around this time. The relatively old ages are not surprising as sample MP10 is of very low metamorphic grade and probably did not experience temperatures greater than about 350°–300°C at any time since deposition. According to the model, final closure took place during a rapid cooling event beginning at ~330 Ma. The age spectrum of MP16 is similar to that of sample MP10, but slightly younger apparent ages are recorded (due to differences in the domain size distribution). This sample began to retain argon at ~390 Ma and the smallest domains closed at ~290 Ma. This model also indicates rapid cooling beginning at ~330 Ma. Results for both MP10 and MP16 are consistent with an isothermal period between ~395 Ma and 330 Ma, at temperatures of 250° and 270°C, respectively.

[27] K-feldspar MP4 is strongly contaminated with excess argon in the first 25% of gas release, but as with both MP10 and MP16, the thermal model indicates a rapid cooling event at ~330 Ma. The latter portion of the age spectrum rises to 400 Ma, which is also consistent with an isothermal period between 390 Ma and 330 Ma, at a temperature of ~260°C.

[28] Samples from these presumed Paleozoic pegmatites show remarkable plateau segments, with age gradients evident only for the first 10–20% of the gas release. For ~85% of the gas released from sample MP6 the apparent ages are in the range 330–335 Ma. The apparent ages decrease to a minimum of ~265 Ma, indicating final closure to argon loss at this time. A very similar age spectrum was obtained for MP1, where the plateau age is ~320–325 Ma, and the youngest apparent age is ~280 Ma. The lack of apparent ages older than 330 Ma raises important questions about the intrusion age of these rocks. Potassium-argon ages of muscovites from these and other Paleozoic pegmatites (MP8, MP5, and MP6) are in the range 360–390 Ma, indicating that emplacement occurred earlier than the apparent ages recorded by the K-feldspars.

[29] Good model fits for the age spectra of MP6 and MP1 are consistent with moderately fast cooling from >350°C at ~330 Ma. However, we caution that these are the highest model temperatures of any of the K-feldspars. Both samples cool at 7.6°C Ma^{-1} between 325 and 300 Ma. In order to account for the absence of ages >340 Ma, we speculate that between the time of intrusion and rapid cooling at 325 Ma, the rocks remained isothermal at a temperature higher than 350°C. Very rapid cooling to ~210°C is required to facilitate closure of all but the smallest diffusion domains at ~325 Ma.

3.4. Interpretation of Hornblende, Muscovite, and Biotite Data

[30] Potassium-argon and $^{40}Ar/^{39}Ar$ ages of the hornblende samples suggest that the highest-grade rocks were at temperatures of at least 500°C until at least ~430 Ma (Figure 6). We suggest that the terrane cooled relatively slowly from the Delamerian through until this time and that the cooling probably accelerated at around 430 Ma, as also suggested by K-feldspar MP10. A second period of accelerated cooling to temperatures below ~350°C followed at around 400 Ma, as indicated by the cluster of muscovite ages within a few million years of 400 Ma. The magnitude of cooling at 430 Ma is difficult to assess, as interpretation of this event is based only on the amphibole data and a single K-feldspar MP10. The magnitude of cooling at 400 Ma

Table 4. Summary of K-feldspar K/Ar and $^{40}Ar/^{39}Ar$ Data

Sample	K/Ar Age, Ma ± 1σ	Integrated Total Fusion $^{40}Ar/^{39}Ar$ Age, Ma ± 1σ
MP24	323.7 ± 2.5	335.8 ± 1.5
MP9	341.3 ± 2.6	338.2 ± 1.4
MP1	323.4 ± 2.5	322.3 ± 1.4
MP6	334.6 ± 2.8	330.0 ± 1.7
MP4	367.2 ± 2.9	375.1 ± 2.0
MP10	388.1 ± 3.1	408.2 ± 1.7
MP16	360.1 ± 3.0	357.7 ± 1.9

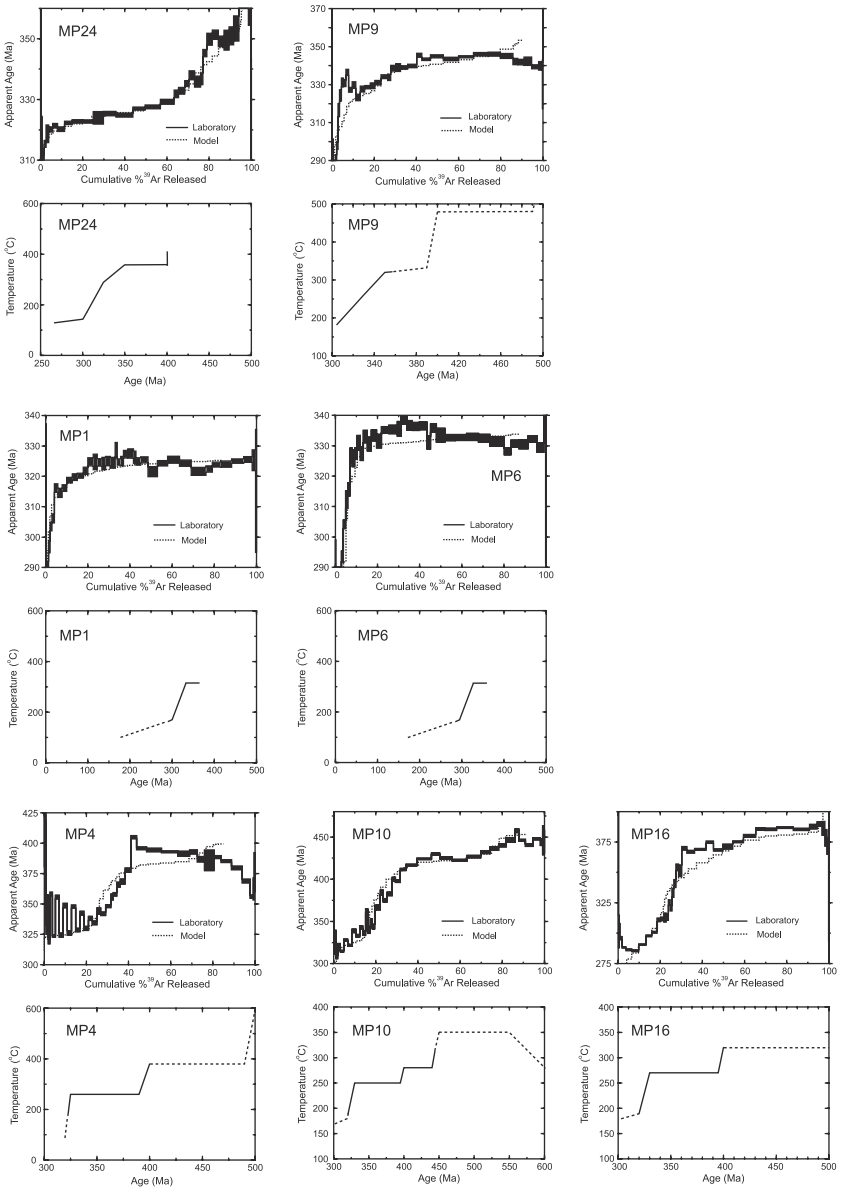

Figure 5. Measured and modeled age spectra and preferred thermal histories for K-feldspar samples. The first figure of each pair shows the calculated age against the fraction of ^{39}Ar released for laboratory and model results. Laboratory results (including 1σ errors in the measured ages) are shown by solid lines; model spectra are shown by dashed lines. The lower figure in each pair shows the temperature-time plot of the preferred thermal histories used to generate the associated model age spectra. Dashed lines indicate where inferred. Diffusion coefficient, relative volume fraction, and relative domain size for each sample are given in the supporting electronic material.

has been assessed, in the remainder of this section, through analysis of argon loss in muscovites and biotites in the interval from ~400 Ma to 330 Ma.

[31] Mica plateau ages are often interpreted to represent the time of closure to argon diffusion. As noted in section 2, this temperature is thought to be ~350°C for muscovite [*Robbins*, 1972; *Dodson and McClelland-Brown*, 1985] and ~300°C for biotite [*Harrison et al.*, 1985]; however, these closure temperatures may vary by as much as 100°C depending on the characteristic diffusion length scale, the activation energy and the cooling rate [*Hames and Bowring*, 1994]. Although the simple closure temperature model is commonly used in the interpretation of mica age data, *Lister and Baldwin* [1996] and *Dunlap* [2000] have shown that if the micas have experienced a long period of residence at near isothermal temperatures slightly below the closure temperature then they are likely to have experienced significant argon loss.

[32] On first inspection the flat age spectra that characterize both muscovite and biotite samples from Mount Painter suggest that the

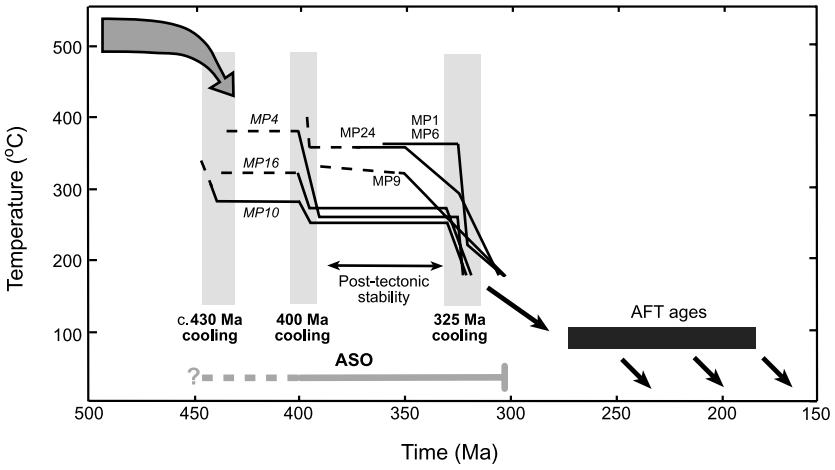

Figure 6. Temperature-time paths for the post-Delamerian history of Mount Painter rocks from various stratigraphic/structural levels (cover samples are italicized). Our interpretation is based on hornblende $^{40}Ar/^{39}Ar$ ages, muscovite K/Ar, and $^{40}Ar/^{39}Ar$ data and multiple-diffusion-domain thermal modeling of K-feldspar $^{40}Ar/^{39}Ar$ data (labeled cooling paths). Slow cooling from the Delamerian metamorphic peak is indicated by the hornblende age data, which, together with K-feldspar MP10, also suggest an episode of accelerated cooling at 430 Ma. A further period of moderately rapid cooling at 400 Ma is suggested by both the muscovite samples (note that the dark arrow indicates the path taken by the deepest, hottest rocks). The amount of cooling during the 325 Ma episode is well constrained by the model fits for the K-feldspar samples, as discussed in the text. Adelaide Fold Belt (AFT) data reported by *Foster et al.* [1994], and the duration of the Alice Springs orogeny in central Australia [*Dunlap and Teyssier*, 1995; *Mawby et al.*, 1999] are also shown.

samples experienced relatively rapid cooling through the closure temperature followed by limited postcrystallization resetting. However, given that step heating of micas does not generally reveal intragrain age gradients, due to homogenization arising from dehydration and structural breakdown of the micas during the experiment [*Gaber et al.*, 1988], and that the best fit thermal histories for the K-feldspar samples reveal a period of isothermal residence between 390 and 325 Ma, it seems appropriate to evaluate the possible contribution of partial argon loss during this period.

[33] In order to do this we have modeled each sample using the method of *Lister and Baldwin* [1996]. A T-t path consistent with hornblende and K-feldspar age data was chosen as a template for the mica modeling. The *Lister and Baldwin* [1996] finite difference algorithm requires that the minerals were completely outgassed prior to being subjected to the model thermal history. In order to ensure this our generic thermal history commenced at very high temperatures (~700°C) at 505 Ma. From this time until 500 Ma we impose rapid cooling to 475°C, followed by slow cooling until around 400 Ma (for simplicity, as none of the micas are likely to have seen the first high temperature cooling event at around 430 Ma). At 400 Ma we impose a second period of rapid cooling, required for the closure of muscovite. This was followed by a second isothermal period between 395 Ma and 330 Ma. The final portion of the thermal history consisted of rapid cooling, between 330 Ma and 325 Ma, and this was well constrained by the results of the MDD modeling of the K-feldspar data. To test the hypothesis of partial argon loss, the temperature during the 395 to 330 Ma isothermal period was varied with the resultant effect on the apparent $^{40}Ar/^{39}Ar$ age noted. This procedure attempted to match the model $^{40}Ar/^{39}Ar$ ages to the measured ages of both biotites and muscovites. For muscovite, diffusion parameters of *Hames and Bowring* [1994] were used, and for biotite, experimental data [*Harrison et al.*, 1985] were used. The diffusion domain size was estimated from the physical grain size.

[34] This modeling revealed two important results. First, partial argon loss during the 395–330 Ma isothermal period does not appear to have significantly affected the muscovite samples. Apparent $^{40}Ar/^{39}Ar$ plateau ages cannot be replicated by varying the temperature of the isothermal period, and we conclude that the muscovite ages reflect nearly complete closure to diffusive argon loss during rapid cooling at ~400 Ma. This conclusion seems valid as many muscovite samples from the basement (MP24, MP9, MP11) and from certain pegmatite samples (MP21, MP5) record K/Ar and integrated $^{40}Ar/^{39}Ar$ ages of ~400 Ma or slightly younger. On this basis we suggest that the rocks must have cooled through the muscovite closure temperature at around 400 Ma, a temperature drop of at least 150°C since around 430 Ma. The younger ages of muscovites MP8 and MP6 may reflect the younger intrusive age of their host pegmatites (Figure 5).

[35] The second point is that partial argon loss does seem to have significantly affected many biotite samples, with modeling showing that minor variations in the temperature of the isothermal period allow all biotite $^{40}Ar/^{39}Ar$ plateau ages to be replicated. Given that the closure temperature of biotite is lower than that of muscovite and that the best fit K-feldspar thermal models place the isothermal residence variably between 350°–250°C, depending on stratigraphic position, it seems likely that significant argon loss in biotite, but not in coexisting muscovite, may have occurred in the isothermal period. This conclusion is also consistent with the wide spread in apparent ages observed for biotite samples not associated

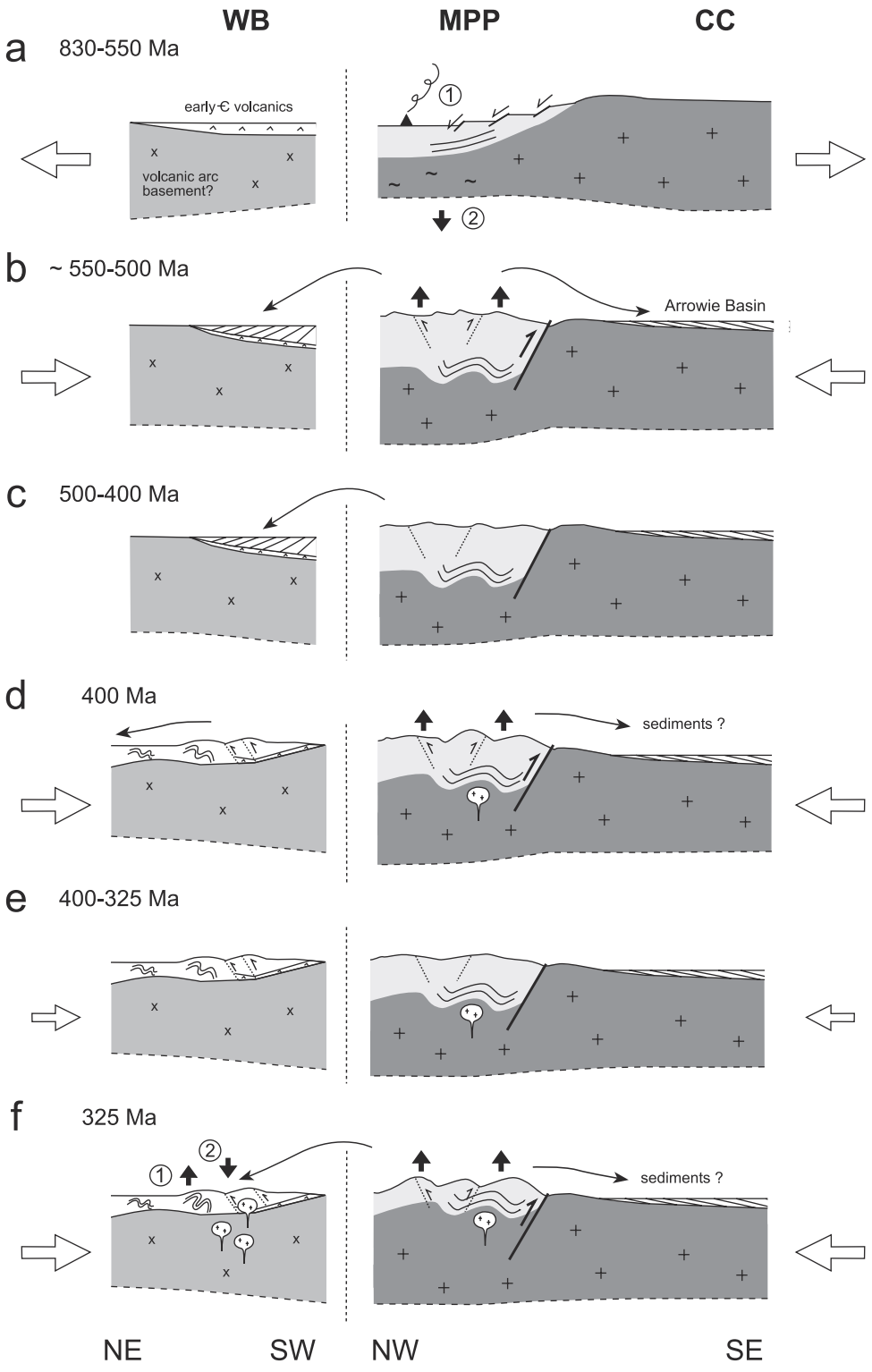
WB
MPP
CC
a
830-550 Ma
early-€ volcanics
volcanic arc basement?
①
②
b
~ 550-500 Ma
Arrowie Basin
c
500-400 Ma
d
400 Ma
sediments ?
e
400-325 Ma
f
325 Ma
①
②
sediments ?
NE
SW
NW
SE

with Paleozoic intrusives. The implications of these results are discussed in section 4.2.

4. Model for the Tectonic Evolution of the Mount Painter Province

[36] Thermal models reconciling hornblende, mica, and K-feldspar age data allow temperature-time paths to be constructed for the rocks at Mount Painter (Figure 6). These thermal models reveal five important periods of the post-Delamerian thermal history: (1) very slow cooling from peak Delamerian temperatures (~500°C) between 500 Ma and around 430 Ma; (2) an increase in the cooling rate at around 430 Ma, probably followed by isothermal residence; (3) a period of moderately fast cooling between 400 and 395 Ma; (4) a period of ~70 Ma during which the terrane was again essentially isothermal; and (5) a third period of accelerated cooling at ~330–325 Ma. The evolution of the MPP and adjacent crustal blocks is summarized in a series of schematic cross sections in Figure 7.

4.1. Delamerian Orogenesis and ~400 Ma Cooling

[37] Hornblende and K-feldspar apparent ages (Tables 2 and 3) suggest a period of accelerated cooling from a temperature of around 475°–450°C at 430 Ma. Unfortunately, this cooling episode cannot be well constrained on the basis of just one K-feldspar sample, but we speculate that it resulted in the final closure of the hornblendes, and was followed by a period of isothermal residence, or very slow cooling, until 400 Ma. At this time the muscovite apparent ages suggest a further period of rapid cooling to temperatures < 350°C. Data from K-feldspars are also consistent with such a cooling episode, although ages of around 400 Ma are recorded only by samples in the uppermost cover sequence. The K-feldspar models provide a constraint on the amount of cooling in this interval and suggest that samples from the cover sequence cooled by up to 65°C, and basement samples by 130°C.

[38] As outlined in section 2, metamorphic evidence suggests that the main fabric (which is axial to the regional mesoscale folds) formed at temperatures in excess of 500°C, implying that the deformation leading to the gross structuring of the Mount Painter region must also have occurred at temperatures >500°C. As hornblende apparent ages are around 430 Ma, the regional scale folding and metamorphism must have occurred prior to 430 Ma. In the absence of higher-temperature thermochronological data, the current data cannot help to constrain the precise timing and duration of peak metamorphism. However, peak metamorphism probably occurred during the Delamerian orogeny (~500 Ma) and was followed by elevated temperatures (near hornblende closure) until around 430 Ma.

[39] As noted earlier, in the absence of a likely source of magmatic heat, *Sandiford et al.* [1998] suggested that the elevated thermal gradients of ~40°C km^{-1} that were associated with peak metamorphism (whether it be Delamerian or slightly younger) simply reflect burial of the high heat-producing Mount Painter basement units beneath the Adelaidean sedimentary cover. If this model is correct, then the presence of such a steady state thermal source allows the amount of exhumation associated with cooling to be constrained, at least to the first order. The thermal models outlined above suggest that the Mount Painter basement rocks cooled by at least 150°C between 430 and 395 Ma. For steady state thermal gradients of around 40°C km^{-1}, this cooling implies around 3–4 km of denudation.

4.2. Posttectonic Stability ~395–330 Ma

[40] Following cooling around 400 Ma, K-feldspar thermal models, for both basement and cover samples, are consistent with a period of posttectonic stability between about 395 and 330 Ma. As outlined in section 3.4, the apparent ages of biotite samples seem to have been affected by partial argon loss during this isothermal (or near isothermal) period. To assess this possibility, we have calculated the maximum temperature that the biotite and K-feldspar samples could be maintained at during this period and still replicate the ages. Interestingly, the estimated paleotemperatures required to replicate the plateau age of the biotite samples show a rough correlation with sample distance from the basement cover unconformity, with samples in the basement recording higher temperatures than samples higher in the cover sequence (Figure 6). Estimates of the gradient yield values in the range 5°–10°C km^{-1} using the biotite model data and/or the K-feldspar MDD models. Although this gradient cannot be constrained with more precision using the samples available in this study, it provides some measure of the lateral thermal gradient along a projected north-south section through the Yankannina anticline and Arkaroola syncline at this time (Figure 3). Given that the mesoscale structuring of the Mount Painter region took place prior to 400 Ma, the presence of such a lateral gradient is intriguing and may be the result of (1) very minor differential exhumation during slight tilting or tightening of the regional folds during subsequent cooling at 325 Ma;

Figure 7. (opposite) NE-SW and NW-SE schematic cross sections showing the Neoproterozoic to Carboniferous evolution of the MPP and adjacent crustal blocks (the Warburton Basin, WB, to the north, and the Curnamona craton, CC, to the southeast). The modern crustal thickness is ~38 km [*Collins*, 1991]. Sediments in the Warburton and Arrowie basins are not shown to scale. Arrows represent inferred tectonic stresses, with size indicating relative magnitude. The Paralana fault is shown as a thick solid line, the other faults in the central portion of the figure shown as thinner lines are inferred structures. (a) Deposition of the Adelaidean sedimentary cover during (1) dominantly rift and sag phase subsidence and (2) dominantly sag phase subsidence. (b) Uplift of the MPP during the Delamerian orogeny was gradual and largely driven by isostatic rebound. (c) Very slow post-Delamerian isostatic rebound, with continued sedimentation in the Warburton Basin. Changing tectonic stresses, potentially related to the earliest ASO, probably caused accelerated cooling at 430 Ma. (d) Exhumation of the MPP during the ASO at 400 Ma; possible intrusion of the British Empire granite and locally derived pegmatites into the middle crust. The MPP was inferred to have been exhumed by at least 3 km from 430 Ma until this time, and the Warburton Basin was deformed under strong compression with folding and thrusting seen throughout the Cambrian and Ordovician sediments. (e) Post-ASO isostatic rebound of the MPP. The region must have been under mild compressive stress, as further deformation is recorded in the Warburton Basin. (f) Final exhumation of the MPP by a further 3 km, with emplacement of the Big Lake granite suite followed by (1) rapid uplift and (2) extension in the Warburton Basin. The Curnamona craton remained essentially stable throughout the Paleozoic history. Evolution of Warburton and Arrowie Basins summarized from *Gravestock* [1995].

or (2) the lateral refraction of heat resulting from the juxtaposition of the high heat-producing Mount Painter basement with the low heat production cover sequence, as suggested by *Mildren and Sandiford* [1995].

4.3. ~330–325 Ma Cooling

[41] The K-feldspar thermal modeling reveals a second period of moderately fast cooling (~4°–8°C Ma^{-1}) commencing between 330 and 325 Ma. During this interval, basement rocks cooled by at least 150°C and samples from the cover sequence cooled by about 100°C. On the basis of the thermal arguments outlined in section 4.1, this cooling is likely to have been associated with a further 3 km of denudation. Pegmatite samples cooled by at least 175°C in the interval between 325 Ma and 300 Ma.

5. Discussion

[42] The new argon age data presented here suggest three periods of post-Delamerian cooling, occurring at 430 Ma, 400 Ma, and ~330–325 Ma, with the 400 Ma and 330 Ma events best identified and constrained by the available data. The 400 Ma and 330 Ma cooling events correlate well with the 400–300 Ma Alice Springs orogeny (ASO), an intraplate tectonic event known throughout central Australia [*Collins and Teyssier*, 1989; *Shaw et al.*, 1992; *Dunlap et al.*, 1995]. The 430 Ma event may also be related to the ASO, on the basis of new geochronological [*Mawby et al.*, 1999] and sedimentological data [*Haines et al.*, 2001] which extend the range of the ASO back as early as 450 Ma. However, the 430 Ma and 400 Ma events also correlate with timing of deformation within the Lachlan orogen in southeastern Australia [*Foster et al.*, 1999], and the 330–325 Ma event may be linked to tectonism in Queensland [*Little et al.*, 1995]. We recognize that much of the tectonism recorded in the Australian continental crust throughout this interval is probably connected, in terms of the stresses related to plate tectonic processes occurring outboard of the eastern continental margin [*Foster et al.*, 1999]. However, given the absence of cooling ages ~330 Ma in the Lachlan orogen, and the absence of 400 Ma deformation in the crustal blocks separating the MPP and the eastern terranes, we prefer to attribute at least the 400 Ma and 330 Ma episodes of cooling observed at Mount Painter to exhumation associated with the ASO. This conclusion is also supported by additional observations, as outlined in the remainder of this section.

[43] The ASO in central Australia exhibits many of the hallmarks of a classic orogeny; these include crustal penetrative thrust systems, large-scale nappe complexes, regional metamorphism and resetting of mineral isotopic systems on a regional scale. Unlike most plate margin orogens there is no significant granite plutonism in the Alice Springs orogen, although localized abundant pegmatite formation supports the notion of limited crustal melting. Metamorphic assemblages developed during the ASO range from subgreenschist to amphibolite facies [*Dunlap et al.*, 1995]. Denudation following Alice Springs deformation in central Australia has resulted in up to 20 km of exhumation which has brought the Proterozoic crystalline rocks of the Arunta Block up from beneath a thick (up to ~8 km) cover sequence of Neoproterozoic and early Phanerozoic sediments forming part of the Centralian Superbasin [e.g., *Korsch and Kennard*, 1991].

[44] Although the central Australian region records the most dramatic evidence for exhumation, deformation, and metamorphism during the Alice Springs orogeny, this event is also recorded in other parts of Australia. In particular, it is seen quite dramatically in the development of the Fitzroy Trough in the northwest of the continent [*Willcox*, 1996]. Additionally, apatite fission track ages from a number of Proterozoic metamorphic terranes surrounding the central Australian region imply that Alice Springs aged tectonism was also associated with mild denudation at the scale of the continent. Examples include the Mount Isa inlier [*Spikings et al.*, 1997] and the Broken Hill region [*Hartley et al.*, 1998]. In the latter case, $^{40}Ar/^{39}Ar$ and apatite fission track analyses reveal Alice Springs aged movement along major regional shear zones. Alice Springs aged tectonism is also recorded in the Darling River lineament system in northwestern New South Wales, where one of three phases of Phanerozoic cooling, ~420–380 Ma, is attributed to this event [*O'Sullivan et al.*, 1998]. Locally, *Gibson and Stüwe* [2000] use apatite fission track data to constrain the exhumation history of the southern Adelaide Fold Belt and suggest that in most areas the terrane cooled from temperatures >120°C in the interval 300–270 Ma. *Gibson and Stüwe* [2000] attribute this cooling to the terminal ASO. Similar Adelaide Fold Belt (AFT) ages of 350–200 Ma were obtained for basement rocks of the Curnamona craton adjacent to the central Adelaide Fold Belt by *Mitchell et al.* [1998]. Although these AFT data suggest that the ASO was associated with minor denudation in the southern Adelaide Fold Belt and adjacent crustal blocks, the argon data described here provide the first evidence to suggest that the ASO was associated with significant denudation anywhere in the Adelaide Fold Belt system.

[45] As the argon data suggest that the ASO was responsible for at least 400°C of cooling at Mount Painter in two pulses at 400 Ma and ~330 Ma, it is likely to have been associated with significant crustal activity in this region at this time. This conclusion is supported by a number of observations. *Idnurm and Heinrich* [1993] have reconstructed paleomagnetic poles for uraniferous breccias in the Mount Gee and Mount Painter regions (Figure 3). These data indicate that the rocks have been magnetized twice, both times during the Permo-Carboniferous. *Idnurm and Heinrich* [1993] note that these reconstructed poles are similar to those published from central Australia, which are generally related to the ASO [e.g., *Li et al.*, 1989], and provide evidence for a hydrothermal fluid flow event through the Mount Painter rocks at this time.

[46] Further evidence is provided by the occurrence of granites in the nearby Warburton Basin (a thin Early Cambrian to Ordovician basin underlying the Cooper Basin; Figure 1) which have been dated by sensitive high-resolution ion microprobe (SHRIMP) analyses on zircons, at 323 ± 5 Ma and 298 ± 4 Ma [*Gatehouse et al.*, 1995]. *Sun* [1997] associates the intrusion of these granites with the first of three major periods of Phanerozoic deformation in the basin. The first event, associated with the ASO, resulted in the intrusion of the granite bodies and the propagation of regional scale thrust faults and large fold structures, the latter resulting in significant internal deformation within the basin. These granites are overlain directly by a thin but continuous sequence of late Carboniferous clastic sediments [*Sun*, 1997], implying that in the interval between 325 and 300 Ma the Warburton Basin area must have been characterized by elevated

geothermal regimes followed by a period of very rapid exhumation in order to unroof these plutons. Erosion of adjacent highlands is also required to provide a source for the dominantly clastic sediments which fill the basin.

[47] The significance of the recognition of Alice Springs aged tectonism at Mount Painter is twofold: (1) It helps constrain the long-term history of the Mount Painter crust, allowing a lengthy history of tectonic reactivation, from the Mesoproterozoic through until the present-day, to be recognized, and (2) it dramatically extends the realm of Alice Springs aged deformation [*Collins and Teyssier*, 1989; *Shaw et al.*, 1992; *Dunlap and Teyssier*, 1995] to the continental scale.

[48] As highlighted in section 1, these points help us understand important questions concerning the factors controlling the distribution of intraplate deformation in the Australian continent. In particular, why did the Mount Painter region suffer much more intense tectonism during this interval than other regions of the Adelaide Fold Belt, or other regions of adjacent Proterozoic crust? What processes controlled the long history of tectonic reactivation, both pre-ASO and post-ASO, which is recorded at Mount Painter? And why has this region suffered repeated tectonic reactivation when other terranes which share a similar history of crustal growth, for example the Mount Isa Inlier, achieved tectonic stability much earlier? The tectonic reactivation in this area during the ASO appears to be a consequence of two factors. First, the thermochronological data presented here show that through most of the Paleozoic, the Mount Painter region was characterized by elevated thermal gradients, almost certainly due to the high concentrations of heat producing elements in the Mount Painter basement rocks [*Sandiford et al.*, 1998]. These thermal gradients resulted in the Mount Painter basement being above ~300°C from the Delamerian orogeny (~500 Ma) through to ~330 Ma, even though for much of this time it was probably at depths significantly shallower than 10 km. The existence of anomalous upper crustal thermal gradients over such long periods of time must reflect conditions appropriate to near steady state conductive geotherms and implies that unusual geothermal conditions extended well down into the lithosphere. Elevated conductive geotherms are expected to equate with dramatic lithospheric weakening, and we propose that the localization of Paleozoic intraplate deformation required to produce the two cooling events documented here, is a primary response to thermally modulated variations in the strength of the Australian continental lithosphere. Second, we suggest that the bounding Paralana fault is linked to a regional scale system of faults to the north that have controlled ASO age deformation not only in the Warburton Basin and central Australia, but also in the Mount Painter region. We suspect that this fault system penetrates into the lithospheric mantle and that ramping along its length was responsible for long-wavelength exhumation of the crust in these regions. This fault system is a persistent zone of weakness that is seismically active today, and the juvenile topography that is clearly seen on aerial photographs of the Mount Painter region suggests this fault system is still effecting exhumation.

Appendix A: Analytical Procedure

[49] Mineral separation was carried out using routine heavy liquid flotation, differential grain size reduction (rolling), and magnetic methods. All samples were concentrated to better than 99%, with the principal impurities being mineral and fluid inclusions. Most K-feldspars were sized between 125 and 180 μm using standard mesh sieves. Most muscovites were sized between 100 and 250 μm (see Tables A1–A12, which are available as electronic supporting material, for details[1]). Hornblendes were sized between 180 and 250 μm.

[50] For the K/Ar analysis, potassium was determined in the samples by dissolving an aliquot of sample overnight in analytical grade 50% weight by weight HF before being diluted to a known volume [e.g., *McDougall and Schmincke*, 1977]. This solution was then analyzed on an Instrumentation Laboratory IL 443 flame photometer, using a lithium internal standard, and the concentration of K (wt %) was determined. A separate aliquot of the sample was fused using an external induction radio frequency generator in an ultrahigh vacuum extraction line. In general, biotite samples were fused at ~1200°–1300°C for 20 min, muscovites at ~1300°–1400°C for 30 min, K-feldspars at ~1500°C for 45 min, and hornblendes at ~1300°C for 30 min. The sample gas was then purified and isotopically analyzed in a MS10 mass spectrometer.

[51] For the $^{40}Ar/^{39}Ar$ analysis, samples were irradiated for 504 hours in facilities X33 or X34 of the Australian Nuclear Science and Technology Organization HIFAR reactor, Lucas Heights, New South Wales. All samples were analyzed at the Australian National University. The sample can was inverted 180° three times during the irradiation to minimize the effect of the large neutron flux gradient along the length of the can; a cadmium liner was used to minimize interference from thermal neutrons. Biotite standard GA1550 (with K/Ar age of 98.8 Ma [*McDougall and Roksandic*, 1974; *Renne et al.*, 1998] was used as the fluence monitor. (See electronic supporting material for further details.)

[52] During step heating experiments the temperature was monitored using a thermocouple at the base of a tantalum crucible within a double-vacuum resistance furnace. The heating schedule for hornblende samples commenced at 800°C to 1450°C; biotite from 550°C to 1350°C; muscovite samples were heated from 700°C to 1350°C, and K-feldspar samples were subject to a series of 43 steps at temperatures between 450°C and 1450°C (including many duplicate or triplicate isothermal steps). The schedules of heating times and temperatures for each sample are listed in the electronic supporting material.

[53] After each temperature step, the gas released was exposed to Zr-Al getters to remove all active gases; gettering time in the vacuum line was generally ~10 min. Subsequently, the purified argon was isotopically analyzed in the mass spectrometer. For micas, isotopic analysis was performed using a VG Isotech MM1200 gas source mass spectrometer, operated in the static mode. Ion beam measurements were made using an electron multiplier with sensitivity of 7.6×10^{-17} mol/mV. For hornblendes and K-feldspars, isotopic analysis was performed using a VG 3600 gas source mass spectrometer. Measurement was made using a Daly detector and a photomultiplier with overall sensitivity 3.5×10^{-17} mol/mV. Corrections for argon produced by interactions of neutrons with K and Ca were made [*Tetley et al.*, 1980]. The ^{40}K abundance and decay constants are taken from standard values

[1] Supporting material is available via Web browser or via Anonymous FTP from ftp://kosmos.agu.org, directory "append" (Username = "anonymous," Password = "guest"); subdirectories in the ftp site are arranged by paper number. Information on searching and submitting electronic supplements is found at http://www.agu.org/pubs/esupp_about.html.

recommended by the International Union of Geological Sciences Subcommission on Geochronology [*Steiger and Jäger*, 1977].

[54] **Acknowledgments.** Our knowledge of the Mount Painter region has benefited from discussions with Eike Paul and Narelle Neumann. Martin Hand is thanked for discussions concerning the Alice Springs orogeny. We thank Jo Mawby, John Mya, Robyn Maier, and Xiaodong Zhang for technical assistance and the Sprigg family for their generosity in allowing access to Arkaroola. Irradiations were undertaken by the Australian Nuclear Science and Technology Organization, through the Australian Institute of Nuclear Science and Engineering. Matt Heizler, Terry Spell, and David Evans provided constructive comments, which significantly improved the manuscript, and we are grateful to Brian Wernicke for his editorial guidance.

References

Bird, P., Kinematic history of the Laramide orogeny in latitudes 35°–49°N, western United States, *Tectonics*, *17*, 780–801, 1998.

Coats, R. P., R. C. Horwitz, A. R. Crawford, B. Campana, and D. Thatcher, Mount Painter Province, 1:125,000 geological map, Geol. Surv. of S. Aust., Adelaide, 1969.

Collins, C. D. N., The nature of the crust-mantle boundary under Australia from seismic evidence, *Geol. Soc. Aust. Spec. Publ.*, *17*, 67–80, 1991.

Collins, W. J., and C. Teyssier, Crustal scale ductile fault systems in the Arunta Inlier, central Australia, *Tectonophysics*, *158*, 49–66, 1989.

Cull, J. P., An appraisal of Australian heat-flow data, *Bur. Min. Res. J. Aust. Geol. Geophys.*, *7*, 11–21, 1982.

De Yoreo, J. J., D. L. Lux, and C. V. Guidotti, Thermal modelling in low-pressure/high temperature metamorphic belts, *Tectonophysics*, *188*, 209–238, 1991.

Dodson, M. H., Closure temperature in cooling geochronological and petrological systems, *Contrib. Mineral. Petrol.*, *40*, 259–274, 1973.

Dodson, M. H., and E. McClelland-Brown, Isotopic and palaeomagnetic evidence for rates of cooling, uplift and erosion, *Geol. Soc. London Mem.*, *10*, 315–325, 1985.

Dunlap, W. J., Natures diffusion experiment: The cooling-rate cooling-age correlation, *Geology*, *28*, 139–142, 2000.

Dunlap, W. J., and C. Teyssier, Paleozoic deformation and isotopic disturbance in the southeastern Arunta Block, central Australia, *Precambrian Res.*, *71*, 229–250, 1995.

Dunlap, W. J., C. Teyssier, I. McDougall, and S. Baldwin, Thermal and structural evolution of the intracratonic Arltunga Nappe Complex, central Australia, *Tectonics*, *14*, 1182–1204, 1995.

England, P. C., Diffuse continental deformation: Length scales, rates and metamorphic evolution, *Philos. Trans. R. Soc. London, 321, Ser. A*, 3–22, 1987.

Foden, J., M. Sandiford, J. Dougherty-Page, and I. Williams, Geochemistry and geochronology of the Rathjen gneiss: Implications for the early tectonic evolution of the Delamerian Orogen, *Aust. J. Earth Sci.*, *46*, 377–389, 1999.

Foster, D. A., J. M. Murphy, and A. J. W. Gleadow, Middle Tertiary hydrothermal activity and uplift of the northern Flinders Ranges, South Australia: Insights from apatite fission-track thermochronology, *Aust. J. Earth Sci.*, *41*, 11–17, 1994.

Foster, D. A., D. R. Gray, and M. Bucher, Chronology of deformation within the turbidite-dominated Lachlan orogen: Implications for the tectonic evolution of eastern Australia and Gondwana, *Tectonics*, *18*, 452–485, 1999.

Gaber, L. J., K. A. Foland, and C. E. Corbato, On the significance of argon release from biotite and amphibole during $^{40}Ar/^{39}Ar$ vacuum heating, *Geochim. Cosmochim. Acta*, *53*, 2457–2465, 1988.

Gatehouse, C. G., C. M. Fanning, and R. B. Flint, Geochronology of the Big Lake Suite, Warburton Basin, northeastern South Australia, *Q. Geol. Notes*, *128*, 8–16, 1995.

Gibson, H. J., and K. Stüwe, Multiphase cooling and exhumation of the southern Adelaide Fold Belt: Constraints from apatite fission track data, *Basin Res.*, *12*, 31–45, 2000.

Gravestock, D. I., The early and middle Paleozoic, in *The Geology of South Australia*, vol. 2, *The Phanerozoic*, edited by J. F. Drexel and W. V. Preiss, *Bull. Geol. Surv. South Aust.*, *54*, 3–61, 1995.

Haines, P. W., M. Hand, and M. Sandiford, Palaeozoic syn-orogenic sedimentation in central and northern Australia: A review of distribution and timing with implications for the evolution of intracontinental orogens, *Aust. J. Earth. Sci.*, *48*, 911–928, 2001.

Hames, W. E., and S. A. Bowring, An empirical evaluation of the argon diffusion geometry in muscovite, *Earth Planet. Sci. Lett.*, *124*, 161–169, 1994.

Harrison, T. M., Diffusion of ^{40}Ar in hornblende: *Contrib*, *Mineral. Petrol.*, *78*, 324–331, 1981.

Harrison, T. M., I. Duncan, and I. McDougall, Diffusion of ^{40}Ar in biotite: Temperature, pressure and compositional effects, *Geochim. Cosmochim. Acta*, *49*, 2461–2468, 1985.

Hartley, M. J., D. A. Foster, and D. R. Gray, The significance of younger thermal events in the Willyama Inliers: Using $^{40}Ar/^{39}Ar$ thermochronology, *Geol. Soc. Aust. Abstr.*, *52*, 19–20, 1998.

Idnurm, M., and C. A. Heinrich, A palaeomagnetic study of hydrothermal activity and uranium mineralization at Mount Painter, South Australia, *Aust. J. Earth Sci.*, *40*, 87–101, 1993.

Jenkins, R. J. F., and M. Sandiford, Observations on the tectonic evolution of the southern Adelaide fold belt, *Tectonophysics*, *214*, 27–36, 1992.

Karlstrom, K. E., and M. J. Williams, A case for simultaneous deformation, metamorphism and plutonism: An example from Proterozoic rocks in central Arizona, *J. Struct. Geol.*, *17*, 59–81, 1995.

Korsch, R. J., and L. M. Kennard (Eds.), Geological and geophysical studies in the Amadeus Basin, central Australia, *Geol. Geophys. Bull.*, 236, 594 pp., Bur. of Miner. Resour., Australia, 1991.

Li, Z. X., C. M. Powell, and P. W. Schmidt, Syn-deformational remanent magnetization of the Mount Eclipse sandstone, Central Australia, *Geophys. J. Int.*, *99*, 205–222, 1989.

Little, T. A., M. O. McWilliams, and R. J. Holcombe, $^{40}Ar/^{39}Ar$ thermochronology of epidote blueschists from the North D'Aguilar Block, Queensland, Australia; timing and kinematics of subduction complex unroofing, *Geol. Soc. Am. Bull.*, *107*, 520–535, 1995.

Lister, G. S., and S. L. Baldwin, Modeling the effect of arbitrary P-T-t histories on argon diffusion in minerals using the MacArgon program for the Apple Macintosh, *Tectonophysics*, *253*, 83–109, 1996.

Lovera, O. M., F. M. Richter, and T. M. Harrison, The $^{40}Ar/^{39}Ar$ thermochronometry for slowly cooled samples having a distribution of diffusion domain sizes, *J. Geophys. Res.*, *94*, 17,917–17,935, 1989.

Lovera, O. M., M. Grove, T. M. Harrison, and K. I. Mahon, Systematic analysis of K-feldspar $^{40}Ar/^{39}Ar$ step heating results, I, Significance of activation energy determinations, *Geochim. Cosmochim. Acta*, *61*, 3171–3192, 1997.

Mawby, J., M. Hand, and J. Foden, Sm-Nd evidence for high-grade Ordovician metamorphism in the Arunta Block, central Australia, *J. Meteorol. Geol.*, *17*, 653–668, 1999.

McDougall, I., and T. M. Harrison, *Geochronology and Thermochronology by the $^{40}Ar/^{39}Ar$ Method*, 2nd ed., 269 pp., Oxford Univ. Press, New York, 1999.

McDougall, I., and Z. Roksandic, Total fusion $^{40}Ar/^{39}Ar$ ages using HIFAR reactor, *J. Geol. Soc. Aust.*, *21*, 81–89, 1974.

McDougall, I., and H.U. Schmincke, Geochronology of Gran Canaria, Canary Islands: Age of shield building volcanism and other magmatic phases, *Bull. Volcanol.*, *40*, 57–77, 1977.

McLaren, S., Long term consequences of the redistribution of heat producing elements within the continental crust: Australian examples, Ph.D. thesis, 172 pp., Adelaide Univ., S. Aust., 2001.

Mildren, S., and M. Sandiford, A heat refraction mechanism for low-P metamorphism in the northern Flinders Ranges, South Australia, *Aust. J. Earth Sci.*, *42*, 241–247, 1995.

Mitchell, M. M., B. P. Kohn, and D. A. Foster, Post-orogenic cooling history of eastern South Australia from apatite fission track Thermochronology, in *Advances in Fission-Track Geochronology*, edited by P. van den haute and F. De Corte, pp. 207–224, Kluwer Acad., Norwell, Mass., 1998.

Neil, E. A., and G. Houseman, Geodynamics of the Tarim Basin and the Tian Shan in central Asia, *Tectonics*, *16*, 571–584, 1997.

Neumann, N. L., Isotopic and geochemical characteristics of the British Empire Granite as indicators of magma provenance and processes of melt generation in the Mount Painter Inlier, South Australia, B.Sc (hons) thesis, 38 pp., Univ. of Adelaide, Aust., 1996.

Neumann, N., M. Sandiford, and J. Foden, Regional geochemistry and continental heat flow: Implications for the origin of the South Australian heat flow anomaly, *Earth Planet. Sci. Lett.*, *183*, 107–120, 2000.

O'Sullivan, P. B., B. P. Kohn, and M. M. Mitchell, Phanerozoic reactivation along a fundamental Proterozoic crustal fault, the Darling River Lineament, Australia: Constraints from apatite fission track thermochronology, *Earth Planet. Sci. Lett.*, *164*, 451–465, 1998.

Paul, E. G., T. Flottmann, and M. Sandiford, Structural geometry and controls on basement-involved deformation in the northern Flinders Ranges, Adelaide fold belt, South Australia, *Aust. J. Earth Sci.*, *46*, 343–354, 1999.

Pollack, H. N., S. J. Hurter, and J. R. Johnson, Heat flow from the Earth's interior: Analysis of the global data set, *Rev. Geophys.*, *31*, 267–280, 1993.

Preiss, W. V., The Adelaide geosyncline: Late Proterozoic stratigraphy, sedimentation, palaeontology and tectonics, *Bull. Geol. Surv. South Aust.*, *53*, 438 pp., 1987.

Preiss, W. V., The Adelaide Geosyncline of South Australia and its significance in Neoproterozoic continental reconstruction, *Precambrian Res.*, *100*, 21–63, 2000.

Renne, P. R., C. C. Swisher, A. L. Deino, D. B. Karner, T. L. Owens, and D. J. DePaolo, Intercalibration of standards, absolute ages and uncertainties in $^{40}Ar/^{39}Ar$ dating, *Chem. Geol.*, *145*, 117–152, 1998.

Richter, F. M., O. M. Lovera, T. M. Harrison, and P. Copeland, Tibetan tectonics from $^{40}Ar/^{39}Ar$ analysis of a single K-feldspar sample, *Earth Planet. Sci. Lett.*, *105*, 266–278, 1991.

Robbins, G. A., Radiogenic argon diffusion in muscovite under hydrothermal conditions, M.Sc. thesis, Brown Univ., Providence, R. I., USA, 1972.

Sandiford, M., M. Hand, and S. N. McLaren, High geothermal gradient metamorphism during thermal subsidence, *Earth Planet. Sci. Lett.*, *163*, 149–165, 1998.

Schaefer, B. F., Isotopic and geochemical constraints on Proterozoic crustal growth from the Mount Painter Inlier, B.Sc (hons) thesis, 29 pp., Univ. of Adelaide, Aust., 1993.

Shaw, R. D., P. K. Zeitler, I. McDougall, and P. R. Tingate, The Paleozoic history of an unusual intracratonic thrust belt in central Australia based on $^{40}Ar/^{39}Ar$, K/Ar and fission track dating, *J. Geol. Soc. London*, *149*, 937–954, 1992.

Sonder, L., and P. C. England, Vertical averages of rheology of the continental lithospheric: Relation to thin sheet parameters, *Earth Planet. Sci. Lett.*, *77*, 81–90, 1986.

Spikings, R. A., D. A. Foster, and B. P. Kohn, Phanerozoic denudation history of the Mount Isa Inlier, Northern Australia: A record of the response of a Proterozoic mobile belt to intraplate tectonics, *Int. Geol. Rev.*, *39*, 107–124, 1997.

Steiger, R., and E. Jäger, Subcommission on geochronology: Convention on the use of decay constants in geo- and cosmochronology, *Earth Planet. Sci. Lett.*, *36*, 359–362, 1977.

Sun, X., Structural style of the Warburton Basin and control in the Cooper and Eromanga Basins, South Australia, *Exp. Geophys.*, *28*, 333–339, 1997.

Teale, G. S., Geology of the Mount Painter and Mount Babbage Inliers, in *The Geology of South Australia*, vol. 1, *The Precambrian*, edited by J. F. Drexel, W. V. Preiss, and A. J. Parker, *Bull. Geol. Surv. South Aust.*, *54,* 93–100, 1993.

Tetley, N., I. McDougall, and H. R. Heydegger, Thermal neutron interferences in the $^{40}Ar/^{39}Ar$ dating technique, *J. Geophys. Res.*, *85*, 7201–7205, 1980.

Wijbrans, J. R., and I. McDougall, Metamorphic evolution of the Attic Cycladic metamorphic belt on Naxos (Cyclades, Greece) utilizing $^{40}Ar/^{39}Ar$ age spectrum measurements, *J. Meteorol. Geol.*, *6*, 571–594, 1988.

Willcox, J. B., Critical tectonic events in the development of the North West Shelf, *Geol. Soc. Aust. Abstr.*, *41*, p. 473, 1996.

Young, G. C., J. R. Laurie, *An Australian Phanerozoic Timescale*, 279 pp., Oxford Univ. Press, New York, 1996.

Zhou, S., and M. Sandiford, On the stability of isostatically compensated mountain belts, *J. Geophys. Res.*, *97*, 14,207–14,221, 1992.

J. Dunlap and I. McDougall, Research School of Earth Sciences, Australian National University, Canberra, ACT 0200, Australia. (jim.dunlap@anu.edu.au; ian.mcdougall@anu.edu.au)

S. McLaren, Research School of Earth Sciences, Australian National University, Mills Road, Acton, ACT 0200, Australia. (sandra.mclaren@anu.edu.au)

M. Sandiford, School of Earth Sciences, University of Melbourne, Melbourne, VIC 3010, Australia. (mikes@unimelb.edu.au)